Highly sensitive D-SPR sensors with optimized metallic thin films for bio-analyte detection.

EHIABHILI, J., PRABHU, R. and KANNAN, S.

2024

photonics

MDPI

Article

Highly Sensitive D-SPR Sensors with Optimized Metallic Thin Films for Bio-Analyte Detection

John Ehiabhili, Radhakrishna Prabhu * and Somasundar Kannan

School of Engineering, Robert Gordon University, Aberdeen AB10 7GJ, UK; j.ehiabhili@rgu.ac.uk (J.E.); s.kannan1@rgu.ac.uk (S.K.)

* Correspondence: r.prabhu@rgu.ac.uk; Tel.: +44-1224262252

Abstract: There is a growing need for precise and rapid detection methods in fields such as biomedical diagnostics, environmental monitoring, and chemical analysis. Surface plasmon resonance (SPR) sensors have been used for the detection and quantification of a wide range of analytes, including biomolecules, chemicals, and gases, in real-time. Despite the promising capabilities of SPR sensors, there remains a gap in creating a balance between having a large enough area to capture a significant number of analytes for detection and being small enough to ensure high sensitivity. This research aims to explore the design of a D-shaped SPR-based optical fiber sensor, focusing on the use of copper, gold, and silver thin films at optimized width and thickness of 10 μm and 45 nm, respectively, to improve the sensor's performance. Employing a computational approach, this study examines the influence of the optimized width and refractive indices of metallic films on the sensor's characteristics. The 10 μm width of the metallic thin film has been found to produce an optimal balance between the sensitivity and the dynamic range of the sensor. Leveraging on the ratio of the real and imaginary parts of the dielectric constant of the thin film metal provides insight into the optical properties and sensitivity at certain wavelengths. Within an analyte refractive index range of 1.37–1.42 and a wavelength range of 650–1200 nm, results indicate that silver outperforms gold and copper at the optimized width with a wavelength sensitivity, and detection accuracy of 12,300 $nmRIU^{-1}$, and 3.075, respectively. By optimizing the width of the metal thin film at 10 μm, a highly sensitive D-SPR is designed, allowing for enhanced sensor detection capabilities for a wide range of bioanalytes.

Keywords: surface plasmon resonance; D-shaped sensor; metal thin film; sensitivity; optical fibre; analyte detection

Citation: Ehiabhili, J.; Prabhu, R.; Kannan, S. Highly Sensitive D-SPR Sensors with Optimized Metallic Thin Films for Bio-Analyte Detection. *Photonics* **2024**, *11*, 764. https://doi.org/10.3390/photonics11080764

Received: 29 June 2024
Revised: 10 August 2024
Accepted: 13 August 2024
Published: 15 August 2024

1. Introduction

Optical fibre sensors are a class of sensors that have attracted a lot of attention due to their versatility, compact size, and ability to operate in a wide range of environments. These sensors exploit the principle of light transmission through optical fibres, which are thin glass or plastic strands that guide light along their length [1]. Hence, they can be engineered to be sensitive to various physical, chemical, and biological parameters, making them suitable for diverse applications, including structural health monitoring, telecommunications, oil and gas, biomedicine, and environmental sensing [2]. Surface plasmon resonance (SPR) is one of the fundamental mechanisms that allows optical fibre sensors to be sensitive to different analytes. SPR is a phenomenon that occurs when light is incident at the interface between a positive and negative permittivity material, causing resonant oscillation of conduction electrons—surface plasmons [3]. SPR is a useful technique for detecting molecular interactions because of its great sensitivity to changes in the refractive index near the sensor surface, which might be influenced by the adsorption of analytes. For SPR to occur, the condition of phase matching between the incident light

and the surface plasmons must be met. This excites the surface plasmons, and energy is transferred, causing a reduction in the reflected light intensity at a specific angle or wavelength, resulting in a dip in the reflected light spectrum [4]. SPR technology has emerged as an essential tool in biomedical research and diagnostics, offering a label-free, real-time, and highly sensitive method for the detection and quantification of biomolecular interactions [5]. SPR technology advancements enable multiplexed platforms for simultaneous analyte detection, accelerating drug discovery, enhancing diagnostics, and studying biomolecular mechanisms, making SPR a key tool in biomedical research and applications [6].

In SPR sensing, the selection of the sensing metal is a critical factor in the design and functionality of the sensor. The metal layer is responsible for supporting the surface plasmon waves that are sensitive to changes in the refractive index near the sensor surface, which occur due to analyte binding [7]. Plasmons are typically stimulated using a laser that matches the requirements for coupling light into the waveguide. The laser light is usually polarized to have a perpendicular component to the metal surface (p-polarized) to excite the surface plasmons. The laser light is coupled into the optical fibre using an optic coupler, which propagates through the fibre and reaches the region where the cladding has been removed and the metal film is deposited. Here, the evanescent field of the guided light interacts with the metal film, which excites surface plasmons at the metal-dielectric interface. Broadband light sources like halogen lamps, supercontinuum lasers, and tunable laser sources can be used for the stimulation of plasmons due to their wavelength variation tendency [8]. The wavelength range used in this research is 650–1200 nm; hence, the light sources stated are applicable. The power can range from a few microwatts to several milliwatts to ensure a sufficient signal-to-noise ratio while avoiding nonlinear effects. The choice of the sensing metal will significantly influence the sensor's performance characteristics, such as sensitivity, stability, and specificity [9]. The most commonly used sensing metals in SPR sensors are gold (Au) and silver (Ag), with each offering distinct advantages and limitations. Deposition techniques such as the electron beam evaporation method, pulsed laser deposition, chemical vapour deposition, and magnetron sputtering can be used to coat the metal on the optical fibre [10]. In some cases, alternative materials like graphene, aluminium (Al), or copper (Cu) might be considered for their unique plasmonic properties, though they are less common than Au and Ag. Additionally, alloying or layering multiple metals can sometimes be employed to combine the advantageous properties of different materials [11].

The incorporation of SPR with optical fibres has been the subject of extensive research due to its potential to create highly sensitive and miniaturized sensors for biomedical applications. Numerous studies have focused on developing SPR-based optical fibre sensors that exploit various fibre geometries, including U-shaped, tapered, and side-polished or D-shaped fibres, to enhance the interaction between the evanescent field and the plasmonic material [12]. The design of the D-shaped optical fibre sensor is a pivotal aspect of its functionality and performance in biomedical applications. The sensor leverages a modified optical fibre, where a portion of the cladding is removed to expose the core, creating a D-shaped profile. This design modification facilitates direct exposure of the fibre core to the external medium, enhancing the interaction between the guided light's evanescent field and the surface plasmons on the metal coating [13]. Recent advancements have demonstrated the use of D-shaped sensors in detecting changes in refractive index, temperature, and the presence of specific chemicals or biomolecules [14].

In the context of D-SPR, many studies have investigated the enhancement of sensitivity by optimizing the thickness of the metallic thin film (40–50 nm). There is no literature on the investigation of sensitivity enhancement due to the width of a metal thin film. Hence, to the best of our knowledge, this is the first study to investigate the width of a metal thin film for improving the sensitivity of a D-SPR sensor. An optimized width and thickness can maximize the interaction between the surface plasmons and the analyte, leading to higher sensitivity and better detection limits. This research work aims to design

a D-shaped SPR sensor that offers high sensitivity by optimizing the width, thickness, and material of the sensing layer. The outcome of this research can lead to the development of highly sensitive, reliable, and versatile sensors suitable for a wide range of applications in healthcare, food safety, environmental monitoring, and chemical analysis. Hence, this sensor technology will provide a balance between sensitivity enhancement and detection accuracy via the optimization of the width of a D-shaped SPR sensor for optical sensing and biomedical applications.

2. Structural Design and Theoretical Simulations

For the geometrical design and numerical simulation of the performance parameters of the sensor, COMSOL Multiphysics software has been utilised. In this research work, a single-mode fibre (SMF) with a 3.1% GeO_2 silica core diameter of 9 μm and a pure silica cladding diameter of 125 μm is used. The 3D schematic diagram of the D-shaped SPR-based optical fibre sensor with coated metal thin film (copper, gold, and silver, respectively) along the axis of the sensor is shown in Figure 1a. Investigating the interaction between the evanescent waves and the external medium is essential for a D-shaped optical fibre sensor. The proposed D-shaped SPR optical fibre sensor can be fabricated through the side polishing technique or laser micro-machining to create a plane sensing area [15]. For the deposition of the metal thin films onto the plane surface of the D-shaped optical fibre, magnetron sputtering or evaporation techniques are utilized. The polishing depth between the etched cladding and the core of the optical fibre (the amount of residual cladding) can be properly controlled [16]. The metallic thin film layer, which serves as the sensing layer, is positioned at a residual cladding distance of D = 0.5 μm from the core of the fibre sensor. The width (w) and thickness (t) of the metal sensing layers were optimized at 10 μm and 45 nm, respectively. Figure 1b illustrates the 2D D-shaped SPR-based fibre design with the design parameters and thin film indicated. A D-shaped biosensor having the above structural parameters is carefully designed to support single-mode operation. Utilizing the Wave Optics Module of COMSOL Multiphysics, the finite element method (FEM) numerical technique investigates the boundary conditions, and mode analysis was used for the study of the 2D sensor design. The refractive indices of the optical fibre core and cladding, the permittivity of the metal layer, and the properties of the surrounding medium are input into the model. The model is then discretized using meshing, which divides the geometry into finite elements that can be used for numerical computation. A physics-controlled extra-fine triangular mesh was utilised to capture the details of the fibre sensor geometry and the plasmonic interactions between the metallic sensing layer and the surrounding medium. To avoid the reflection of any incident waves, regardless of their angle or frequency, an artificial absorbing layer known as a perfectly matched layer (PML) is designed to surround the simulated region. To inject an analyte into the structure, a microfluidic channel or flow cell can be integrated with the sensor. The microfluidic channel is positioned over the D-shaped region of the fibre sensor, allowing the analyte to flow directly over the metal film where the SPR occurs [17]. The analyte solution is then introduced into the channel inlet using a pump system. The analytes may be protein, glucose, heavy metals in the water sample, toxins, viruses or bacteria in the samples. However, the desired analytes in this research are viruses. To simulate the sensor's interaction with biological analytes, the refractive index at the sensor surface is varied to represent the binding of biomolecules. This allows for the simulation of changes in the SPR signal due to molecular interactions and the assessment of the sensor's sensitivity. Parameter studies are conducted to analyse the sensor's performance under various conditions. This includes sweeping through a range of wavelengths, refractive indices, and geometric parameters to explore their effects on the SPR response. The simulations help identify the optimal sensor design and operational parameters.

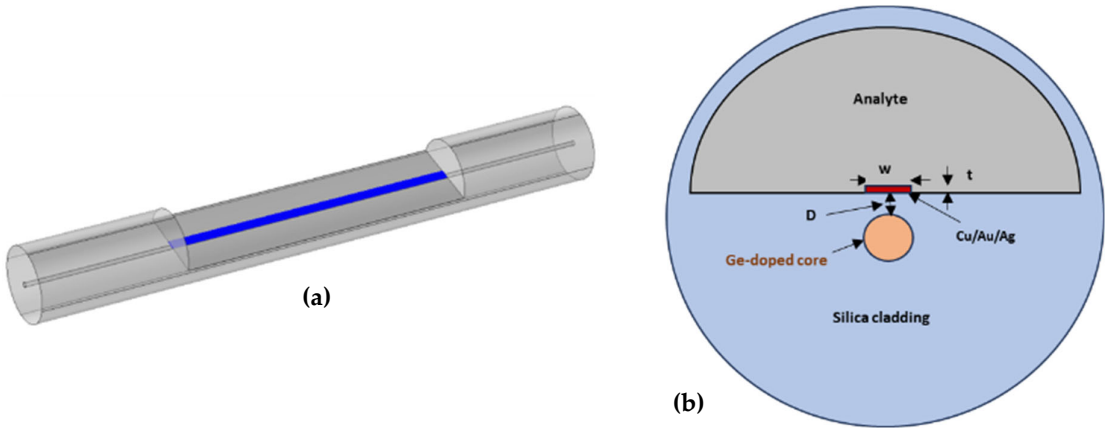

Figure 1. (**a**) 3D schematic of D-SPR sensor; (**b**) 2D sensor design showing the design parameters.

All fibre-based SPR sensors rely on the coupling between the core mode and the surface plasmon polariton mode under phase-matching conditions. This initiates a resonance condition, which is seen as a dip in the sensor's transmission curve. This phase-matching condition is expressed as [18]:

$$k_{SP} = \frac{\omega}{c}\left(\frac{\in_m \in_d}{\in_m + \in_d}\right)^{1/2} \quad (1)$$

where k_{SP} is the surface wave vector, ω is the angular frequency, c is the speed of light in vacuum, $\in_m$ and $\in_d$ are the permittivity of the metal and dielectric, respectively.

The refractive index of the silica cladding and Ge-doped core are determined using the Sellmeier equation expressed as [19]:

$$n^2(\lambda) = 1 + \frac{a_1\lambda^2}{\lambda^2 - C_1^2} + \frac{a_2\lambda^2}{\lambda^2 - C_2^2} + \frac{a_3\lambda^2}{\lambda^2 - C_3^2} \quad (2)$$

where λ is the incident light wavelength in μm; n is the wavelength-dependent refractive index of the fibre core and cladding. $a_1, a_2, a_3, C_1, C_2,$ and C_3 are Sellmeier constants given in Table 1 [19].

Table 1. Sellmeier constants for fibre core and cladding.

Constants	a_1	a_2	a_3	C_1 (μm)	C_2 (μm)	C_3 (μm)
Silica cladding	0.6961663	0.4079426	0.8974794	0.0684043	0.1162414	9.896161
Ge-doped core	0.7028554	0.4146307	0.8974540	0.0727723	0.1143085	9.896161

The dielectric function of a metal layer is determined using the Drude-Lorentz model and is expressed as [20]:

$$\varepsilon_m(\omega) = \varepsilon_\alpha - \frac{\omega_D^2}{\omega^2 + i\gamma\omega} + \Delta\varepsilon_p \frac{\boldsymbol{\Omega}_p^2}{\boldsymbol{\Omega}_p^2 - \omega^2 - i\boldsymbol{\Gamma}_p\omega} \quad (3)$$

where ω_D is the plasma frequency, γ is the damping coefficient, $\Delta\varepsilon_p$ is the weighting coefficient, Ω_p is the oscillator strength, Γ_p is the spectral width, and ε_α is the interband offset for the metal [21]. The values of the Drude-Lorentz model parameters are given in Table 2 [22].

Table 2. Drude-Lorentz model parameter values.

Parameters	Ag Thin Film	Au Thin Film	Cu Thin Film
ε_α	1.55	3.5	1.25
ω_D(PHz)	2.176	2.169	1.985

γ(THz)	16.93	7.254	7.254
$\Delta\varepsilon_p$	1.0	0.35	1.39
Ω_p(PHz)	1.39	0.648	0.7133
Γ_p(PHz)	0.6529	0.1086	0.2587

The confinement loss, L_c, is calculated in dB/m using the following expression [23]:

$$L_c = 8.686.\frac{2\pi}{\lambda}.I_m(n_{eff}) \quad (4)$$

where $I_m(n_{eff})$ is the imaginary part of the effective refractive index, which is related to the attenuation or absorption of light as it propagates through the material medium. The transmission coefficient, T, can be expressed as [24]:

$$T = \exp\left(\frac{4\pi}{\boldsymbol{\lambda}}.(n_{eff})_{imag}.L\right) \quad (5)$$

where L is the length of the sensing region. An important parameter is the sensor's sensitivity. *Sensitivity* of a sensor is the degree of response to a change in an input signal. Sensitivity refers to the sensor's ability to detect small changes in the refractive index of the surrounding medium, which corresponds to the detection of low concentrations of analytes. Wavelength sensitivity is given as [25]:

$$S_\lambda(nm/RIU) = \frac{\Delta\lambda_{peak}}{\Delta n_a} \quad (6)$$

where $\Delta\lambda_{peak}$ is the peak shift in resonant wavelength and Δn_a is the change in the analyte's RI. Amplitude sensitivity, which refers to the change in the intensity of the transmitted light because of changes in the analyte RI in contact with the sensor, is given as [25]:

$$S_A(RIU^{-1}) = -\frac{1}{\alpha(\lambda, n_a)}\frac{\delta\alpha(\lambda, n_a)}{\delta n_a} \quad (7)$$

where $\alpha(\lambda, n_a)$ is the loss/attenuation and $\delta\alpha(\lambda, n_a)$ is the change in the loss spectrum resulting from the change in analyte RI.

Limit of Detection (LOD) is defined as the smallest quantity or concentration of an analyte that can be reliably detected by the sensor. The LOD is a critical parameter in biomedical sensing, where analytes may be present at very low concentrations.

Resolution is a measure of a sensor's ability to detect a minimum RI change in the surrounding medium. It is expressed as [26]:

$$R\ (RIU) = \frac{\Delta n_a\ \times\ \Delta\lambda_{min}}{\Delta\lambda_{peak}} \quad (8)$$

Figure of merit (FOM) and detection accuracy (DA) are measures of a sensor's performance obtained by combining its sensitivity, resolution, and dynamic range. It is calculated thus [26]:

$$FOM = \frac{S_\lambda}{FWHM} \quad (9)$$

$$DA = \frac{\Delta\lambda_{res}}{S_\lambda}\ .\ FWHM \quad (10)$$

where FWHM is the full width at half-maximum of the spectra.

3. Results and Discussion

This study presents comprehensive theoretical modelling results for the optimized width and thickness of metal thin films for D-shaped SPR optical fibre sensors. The geometry of the D-shaped optical fibre sensor, including the metallic thin film width and

thickness, and the length of the polished area can be optimised to maximise the overlap between the evanescent field and the plasmon field, enhancing sensitivity. Employing COMSOL Multiphysics software, the performance of sensors with a 10 µm width metal film was simulated, incorporating a 500 nm residual cladding and a thickness layer of 45 nm.

Cu, Au, and Ag were each coated on the flat surface of the D-shaped fibre sensor, and each was subject to different sensing performance measurement for analyte detection. Investigative analysis was carried out using an analyte RI range of 1.37–1.42. This falls within the range of the refractive index of most viruses and certain biomolecules. However, this research is intended for detecting the presence of viruses in biological samples.

The transmission spectrum of the phase match between the core and SPP mode of the D-shaped SPR sensor is shown in Figure 2. The grey line represents the transmission spectrum of the SPR sensor at an analyte refractive index of 1.42. The insets in Figure 2 show the electric field coupling of light between the metallic thin film and the core of the optical fibre. The electric field at the metal-dielectric interface is strengthened when energy is transferred from the core of the fibre to the interface. SPR is primarily excited by p-polarized waves because the electric field component of the p-polarized light can induce surface plasmons at the metal-dielectric interface. The x-orientation of the p-polarized wave has been considered because the electric field vector of the p-polarized light has a significant component normal to the metal surface when oriented along the *x*-axis. The peak is the fundamental plasmonic mode, and it occurs at the resonant wavelength due to the interaction of the evanescent field with the metallic-thin film's surface electrons. This mode is known as surface plasmon polariton (SPP) mode in the context of a planar surface or guided mode in the context of waveguides like optical fibre. This mode involves the propagation of light through the fibre core, generating an evanescent field that extends into the cladding and interacts with a metallic layer deposited on the cladding. When the conditions for SPR are met, this interaction excites surface plasmons that propagate along the metal-dielectric interface. This mode is the most sensitive to changes in the refractive index of the surrounding medium and is thus critical for sensing applications. The fundamental mode peak is typically used for sensing due to its high sensitivity.

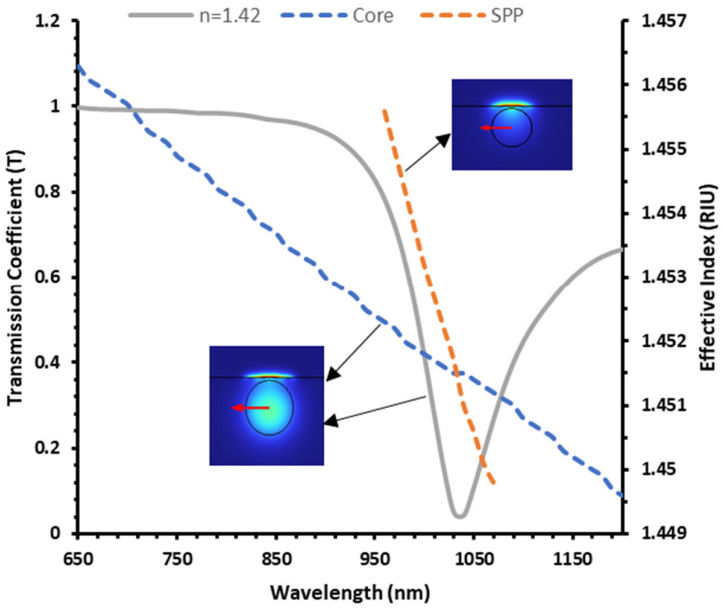

Figure 2. Phase matching between core and SPP mode of D-shaped sensor.

Figure 3a shows the graph of the transmission spectra of Ag thin film for 35 nm, 40 nm, 45 nm, 50 nm, and 55 nm thickness, respectively. The dip in the transmission spectrum indicates the excitation of surface plasmons, which occurs when the momentum of the incident light matches the momentum of the surface plasmons at the metal-dielectric interface. The depth of the dip is a measure of the efficiency of this excitation process. A deeper dip typically indicates a more efficient excitation of surface plasmons, suggesting better sensitivity for sensing applications. As the thickness of the silver thin film changes, the wavelength needed to satisfy the phase matching condition also changes, leading to a shift in the SPR dip wavelength. Thus, at a metal thin film thickness of 45 nm, the coupling efficiency between the light and surface plasmons for this sensor configuration is maximized. From Figure 3b, the residual cladding distance D affects the interaction between the evanescent field of the light propagating through the fibre core and the plasmons at the metal-dielectric interface. The intensity of the evanescent field decays with distance from the fibre core. A smaller D allows for a stronger interaction between the field and the metal film, potentially leading to a more efficient excitation of surface plasmons and a deeper dip in the transmission spectrum. However, a smaller D might lead to significant absorption and damping of the plasmons due to the proximity of the metal film to the fibre core, potentially reducing the interaction length and affecting the sensor's performance. Conversely, a larger D could result in a weaker evanescent field interaction, reducing sensitivity. In addition, the choice of D must also consider practical fabrication and stability issues to ensure a reliable sensor design. Hence, the residual cladding was optimized at 0.5 μm. Figure 4a illustrates the relationship between the wavelength at RI = 1.42 and transmission spectra in terms of the distinct width of Ag thin film. As the width increases, a remarkable dip in SPR is produced, thereby increasing the plasmonic effect. However, for a metal thin film width ≥ 10 μm, the transmission spectra are almost unchanged. The lateral extent of the evanescent field and the associated sensing capabilities are not significantly enhanced by further increases in the thin film width at these dimensions. Figure 4b shows the sensitivity of the sensor for different Ag thin film widths for a refractive index change from 1.41 to 1.42. As the width increases, the sensitivity increases. However, increasing the width of the Ag thin film beyond 10 μm results in a non-significant change in the sensitivity of the sensor. This can be attributed to light confinement within the fibre core in a single-mode regime. The interaction between the guided light and the metal thin film is maximized under this condition. Increasing the width of the thin film beyond a certain point does not significantly alter this interaction because the light remains confined within the core, and the effective area of interaction with the metal surface does not change appreciably. Hence, the width of the metal-thin film has been optimized at 10 μm.

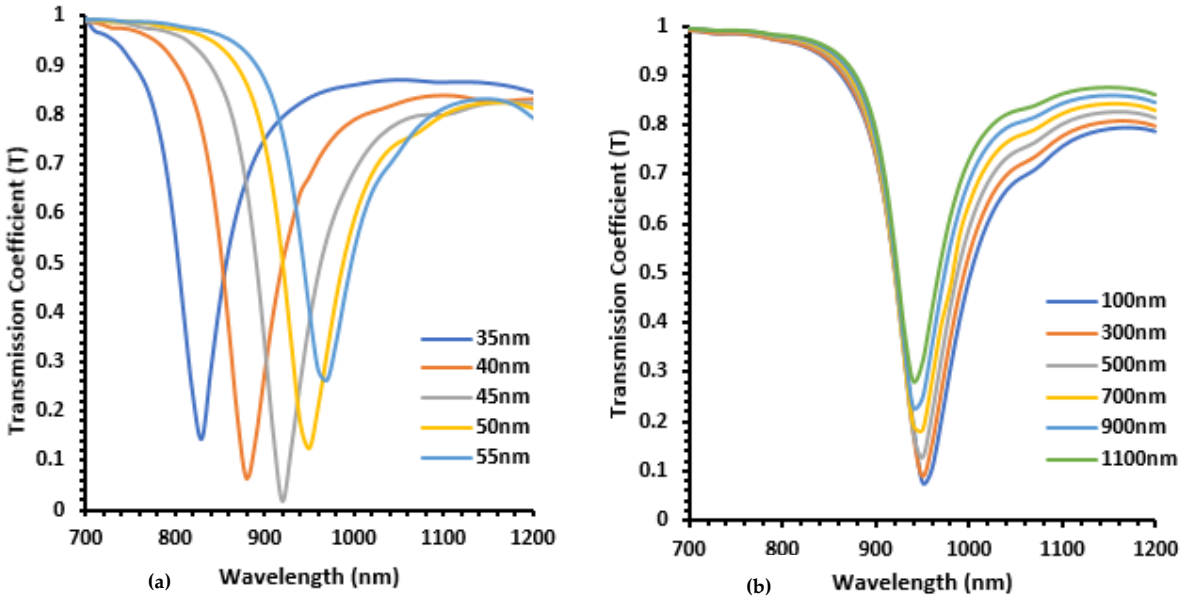

Figure 3. Transmission spectra for different (**a**) thicknesses of Ag thin film; (**b**) residual cladding thickness (D) of sensor design.

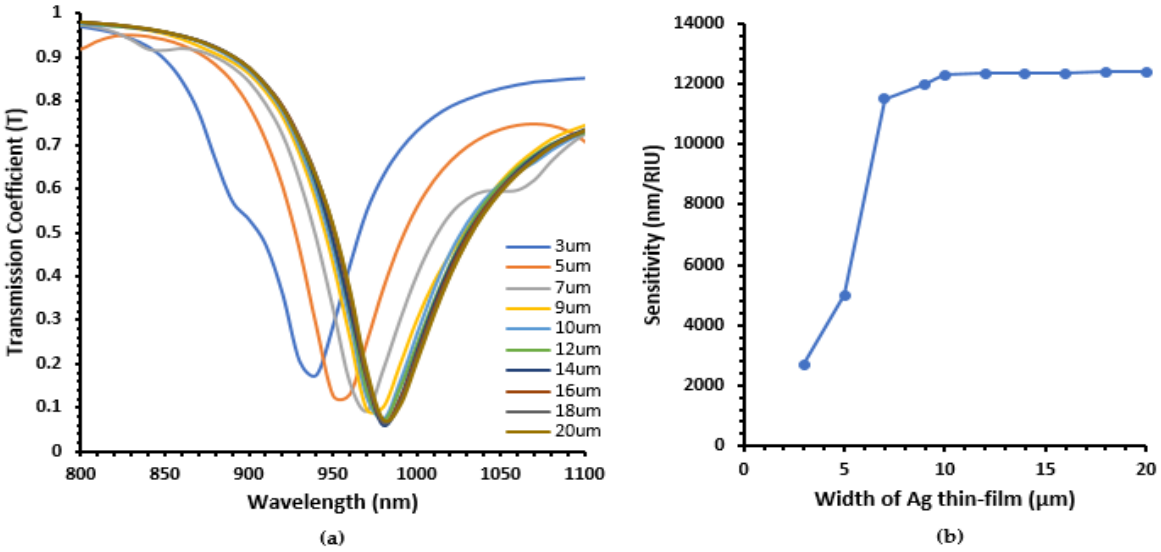

Figure 4. (**a**) Transmission spectra at RI = 1.42 and specific Ag widths; (**b**) Graph of sensitivity against specific Ag thin film widths of analyte RI from 1.41 to 1.42.

To understand the effect of the different metal coatings (Cu, Au, and Ag) on the D-shaped SPR sensor, the transmission spectra are plotted. Figure 5a–c shows that with increasing analyte RI (from 1.37 to 1.42) for the three-metal thin films, the SPR curve moves towards longer wavelengths, with gold showing a greater red shift compared to copper and silver. At RI of 1.42, the peak wavelengths of copper, silver, and gold were 973 nm, 977 nm, and 1035 nm, respectively. This is due to the differences in the properties of the materials. Gold has a larger free electron density and dielectric constant compared to silver and copper, leading to larger shifts in the peak wavelength [27]. Also, when the analyte refractive index increases, the resonance condition for SPR shifts because the change in refractive index alters the speed of light within the medium and, consequently, the momentum matching conditions between the incident light and the surface plasmons. This

shift is due to the increased optical path length that results from a higher analyte refractive index. Figure 5d shows the nonlinear changes in the peak wavelength of the different sensors. This shows that the resonance between the core and SPP mode increases gradually with increasing analyte RI. The graph of the thin film refractive index against the wavelength using the Drude-Lorentz model is shown in Figure 6a. From the figure, silver has the lowest real part of refractive index (n) across the wavelength range. This results in a higher penetration depth of the evanescent field into the analyte region, allowing for a larger interaction volume and potentially higher sensitivity. The imaginary part of the refractive index (κ) indicates optical losses and affects the sharpness and sensitivity of the SPR signal. In the wavelength range, gold has a lower κ, indicating less absorption of light and a longer propagation length of surface plasmons. The ratio $^{n}/_{\kappa}$ provides insight into the metal's optical properties. From Figure 6b, silver shows a high $^{n}/_{\kappa}$ ratio, implying that it supports SPs with lower propagation losses. However, for wavelengths of about 1000 nm and above, gold has a greater $^{n}/_{\kappa}$ ratio. This is because at these wavelengths, the κ part became significantly higher than the n part, contributing to higher optical losses.

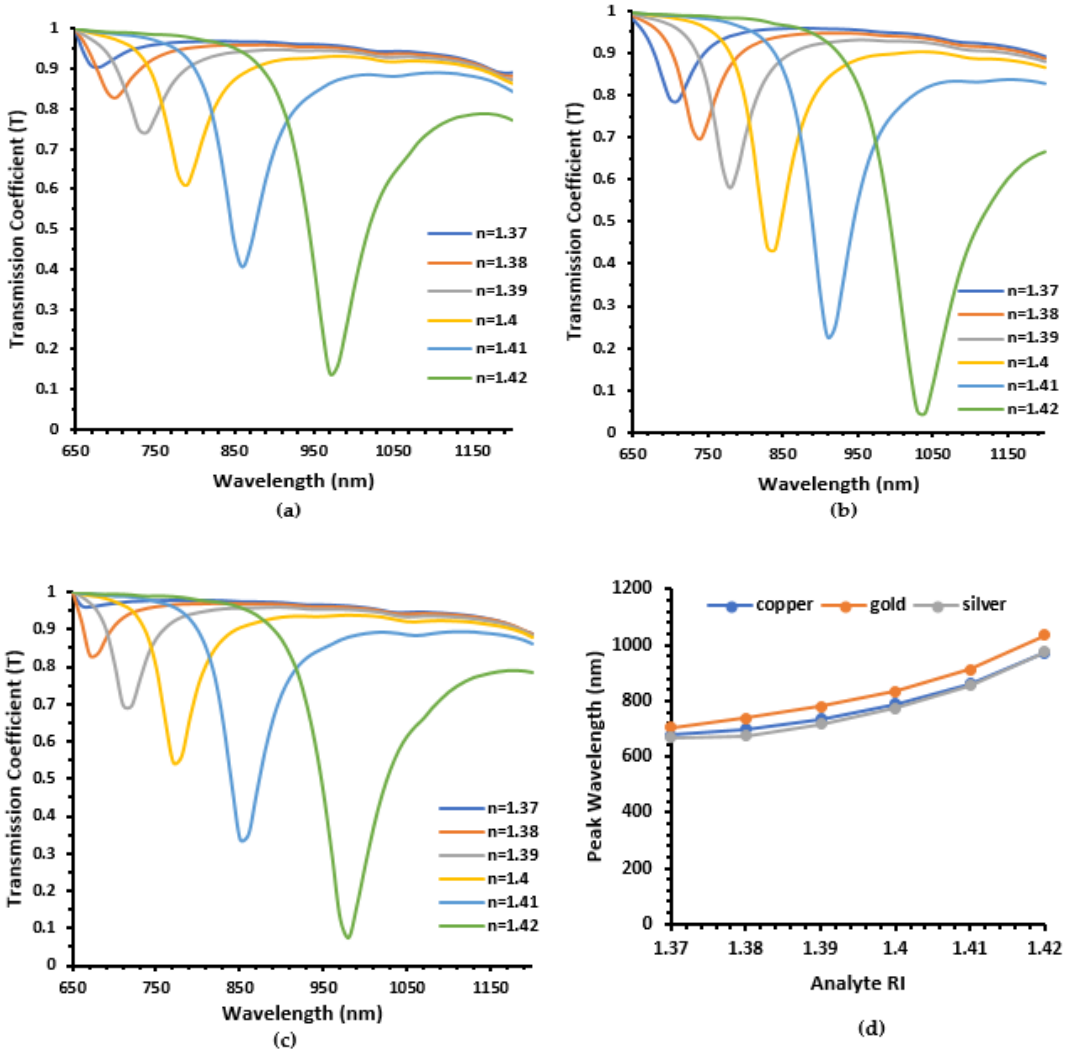

Figure 5. Transmission spectrum for (**a**) copper; (**b**) gold; (**c**) silver; (**d**) Peak wavelength as a function of analyte RI from 1.37 to 1.42.

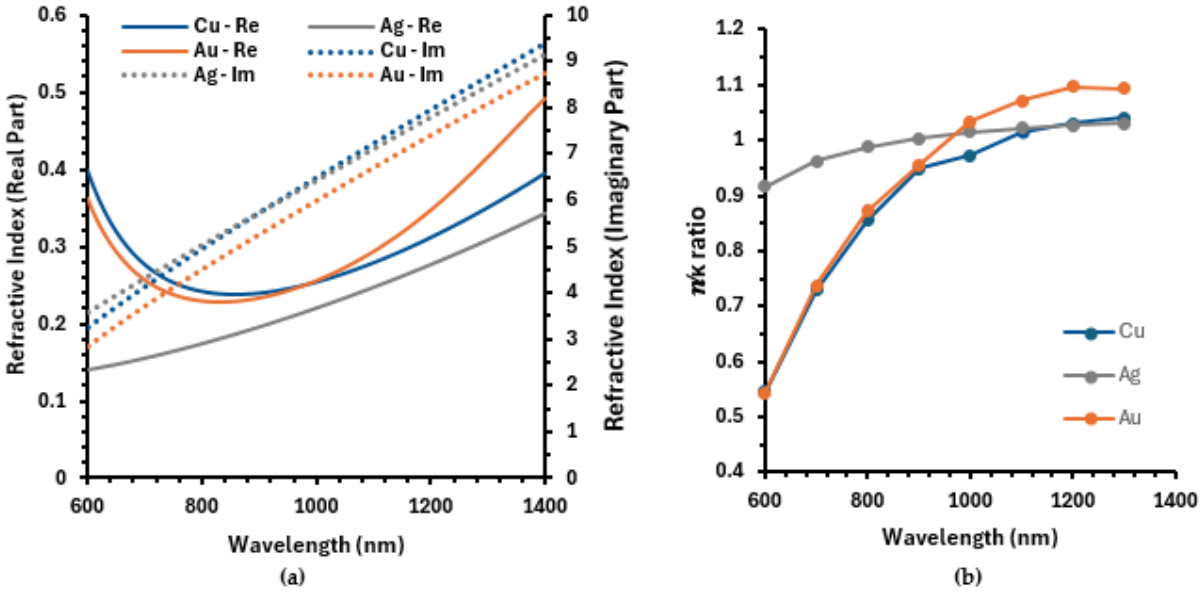

Figure 6. Graph of (**a**) real and imaginary refractive index against wavelength; (**b**) $^{n}/_{\kappa}$ against wavelength

Figure 7a–c shows the graph of the confinement loss against wavelength for copper, gold, and silver thin films, respectively. As the refractive index increases, the interaction between the guided light and the analyte changes, potentially leading to changes in the resonance conditions, deeper penetration of the evanescent field, redistribution of the optical power, and increase in absorption at the wavelength of the guiding light. All these can contribute to confinement loss increase, leading to a significant reduction in the amount of light reaching the detector, thus reducing the sensitivity. In practical situations, a high loss can degrade the SNR of the sensor design, making it more difficult to distinguish the signal from background noise. However, this loss can be minimized by developing signal processing techniques to improve the SNR. This graph, for a D-shaped optical fibre SPR-based sensor, is directly related to the amplitude sensitivity of the sensor. The height of the peak indicates the strength of the SPR interaction. For analyte RI of 1.42, silver showed the highest amplitude sensitivity of 1932.51 RIU^{-1}. For the same analyte RI, gold and copper showed amplitude sensitivities of 1454.56 RIU^{-1} and 1224.25 RIU^{-1}, respectively. The peak characteristics and the noise level in the graph are critical for assessing how effectively the sensor can detect changes in the surrounding refractive index, which is essential for applications like biosensing, chemical detection, and environmental monitoring.

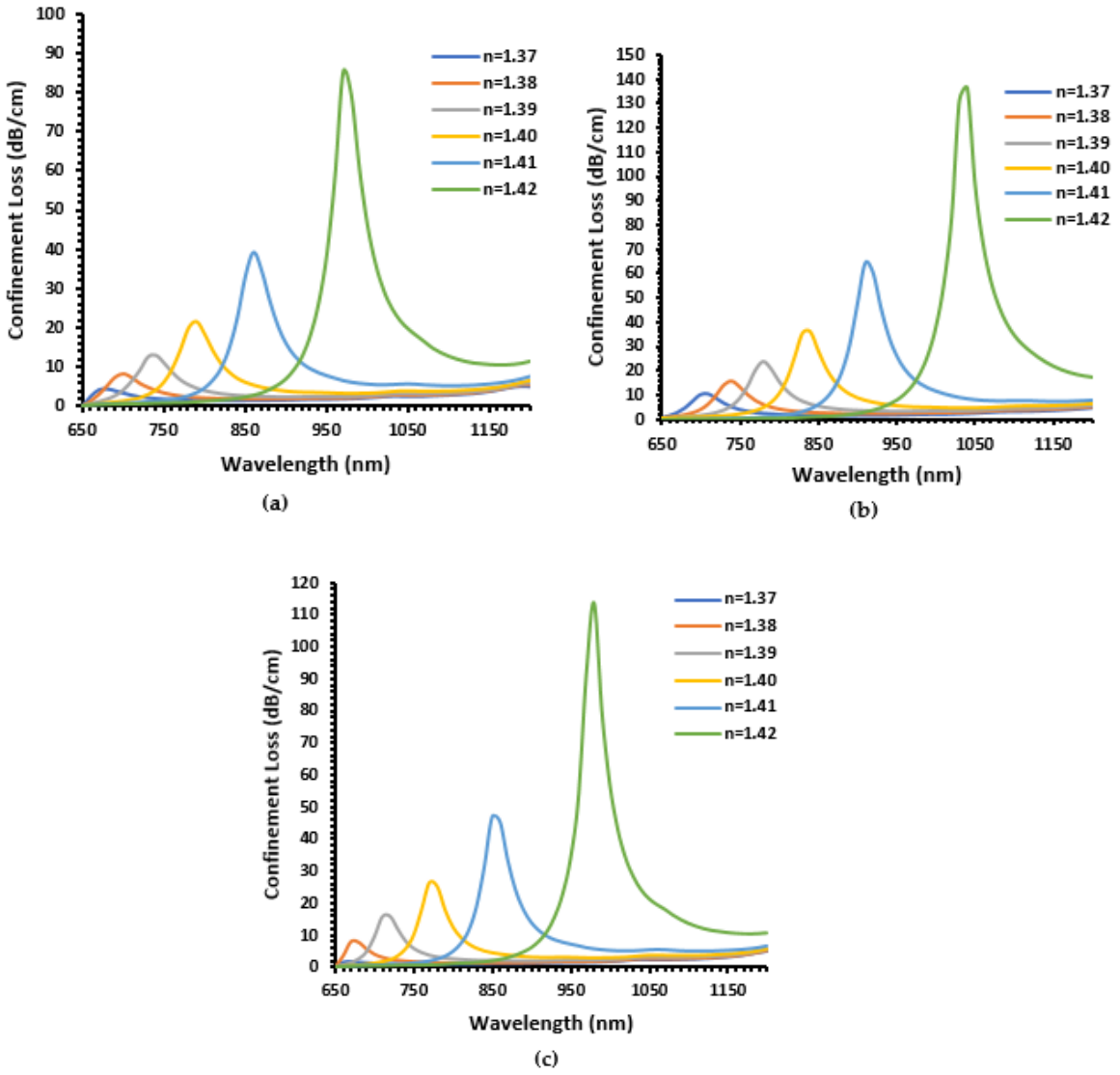

Figure 7. Confinement loss spectra for (**a**) copper; (**b**) gold; (**c**) silver thin film D-SPR sensor.

Figure 8a depicts the graph of the wavelength sensitivity of the three sensor designs against the analyte refractive index. From the graph, silver has the highest wavelength sensitivity of 12,300 nmRIU^{-1} at analyte RI of 1.42, slightly better than that of gold with a wavelength sensitivity of 12,200 nmRIU^{-1}. Copper has the least wavelength sensitivity at the same RI, with 11,300 nmRIU^{-1}. This is because silver has the highest plasma frequency and the lowest optical losses in the visible and near-infrared regions among the three metals, resulting in a more pronounced and sharper SPR resonance curve, which translates to higher wavelength sensitivity. This means that small changes in the refractive index of the surrounding medium will cause a relatively large shift in the resonance wavelength, making silver an excellent choice for high-sensitivity applications. Although copper is outperformed by silver and gold thin films, it can be used in designs and specific applications where cost is a high consideration. However, silver has the tendency to oxidize and tarnish, especially when exposed to air and various chemical environments, posing a significant challenge for its practical application in sensor technologies. Applying a thin protective layer over the silver can shield it from the environment, thereby preventing or significantly slowing down the oxidation process. Materials such as graphene, silicon dioxide,

or specific polymers can serve as effective protective coatings. Figure 8b shows the plot of FWHM against the analyte RI. The FWHM represents the width of the SPR resonance peak at half of its maximum intensity and is a measure of the spectral resolution and quality of the resonance. For the analyte RI considered in the design, silver showed a smaller FWHM compared to gold and copper, which indicates a sharper resonance peak. This generally corresponds to higher sensor resolution and the ability to discriminate between small changes in analyte RI. Typically, the performance of a sensor is enhanced when the sensitivity increases with a decrease in FWHM [21]. High resolution often leads to higher detection accuracy (DA), as the sensor can more precisely locate the resonance condition.

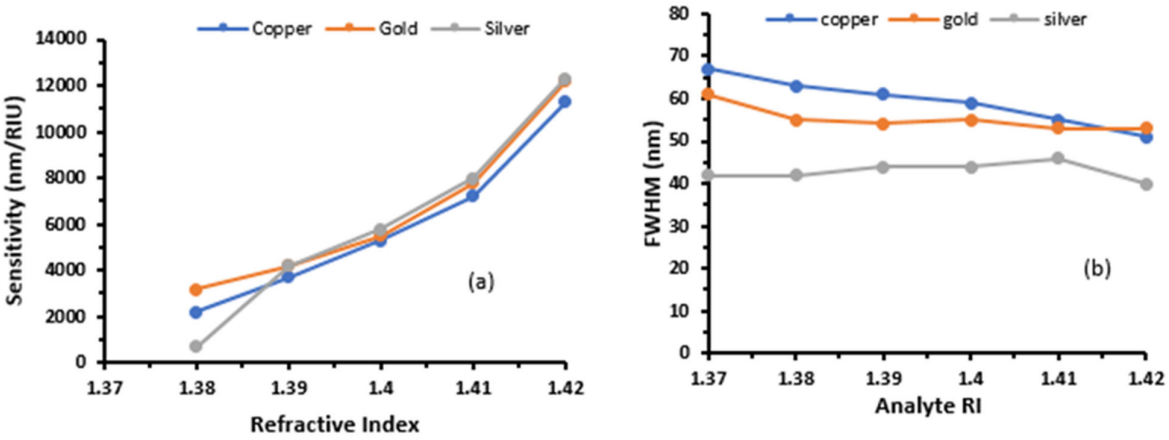

Figure 8. (**a**) Wavelength sensitivity graph; (**b**) Graph of FWHM against analyte RI.

Table 3 gives a comparison of the performance metrics for copper, gold, and silver thin film D-shaped SPR-based optical fibre sensors for analyte RI of 1.42. From the table, silver performed better than gold and copper, showing a higher wavelength and amplitude sensitivity, narrower FWHM, better FoM, resolution, and DA for a RI of 1.42.

Table 3. Comparison of Cu, Au, and Ag SPR sensor performance metrics.

	S_λ (nm/RIU)	S_A (RIU^{-1})	FWHM (nm)	FoM (RIU^{-1})	Resolution (RIU)	DA
Copper	11,300	1224.25	51	221.57	8.85×10^{-6}	2.216
Gold	12,200	1454.56	53	230.19	8.20×10^{-6}	2.302
Silver	12,300	1932.51	40	307.50	8.13×10^{-6}	3.075

The increased wavelength and amplitude sensitivity for the metal thin films as analyte RI increases is due to the increased electric field intensity at the metal-dielectric interface. To fabricate these sensors, a trade-off in wavelength sensitivity, spectral resolution, and sensor geometry must be considered for specific application requirements. A comparison of this design with existing designs from literature is presented in Table 4.

Table 4. Comparison of the performance of this D-shaped Cu, Au, and Ag optical fibre SPR sensor with other optical sensors published in literature.

Ref	Sensor Configuration	Sensing Material	Operating Wavelength (nm)	RI Range	Wavelength Sensitivity (nm/RIU)	Amplitude Sensitivity (RIU^{-1})	Resolution (RIU)
[28]	Spiral PCF-SPR	Gold	-	1.33–1.38	4600	420.4	2.17×10^{-5}
[29]	External coated PCF SPR	Gold	2550–2900	1.23–1.29	5500	333.8	7.69×10^{-6}
[30]	Hollow-core PCF	Gold	1078–2097	1.27–1.45	5653.57	590	-
[31]	Hollow-core PCF	Silver	500–800	1.33–1.37	4200	300	2.38×10^{-5}
[32]	D-shaped PCF	Gold	2900–3600	1.33–1.39	11,500	230	8.7×10^{-6}
[33]	Ag coated PCF SPR	Silver	-	1.33–1.42	11,000	1420	9.1×10^{-6}
[34]	Solid core MOF	Gold	770–850	1.36–1.39	7000	886.9	4×10^{-5}
	This work	Silver	650–1200	1.37–1.42	12,300	1932.51	8.13×10^{-6}
		Gold			12,200	1454.46	8.2×10^{-6}
		Copper			11,300	1224.25	8.85×10^{-6}

This research study considers a uniform distribution of analytes for the specified refractive index range. A non-uniform distribution of analytes means that the refractive index of analytes varies across the sensing area. This variation can affect how the evanescent field of the guided light interacts with the analytes. Since sensitivity and resonance conditions are highly dependent on the local refractive index at the sensor surface, a nonuniform distribution could lead to a broader or multi-modal response, requiring a different approach and possibly modifications in the sensor design to maintain sensitivity and accuracy.

4. Conclusions

D-shaped optical fibre SPR-based sensors have diverse advantages and are widely employed due to their high sensitivity and ease of integration with other devices. The theoretical investigation into the sensing parameters of different metallic thin films of D-shaped SPR optical fibre sensors, as presented in this study, has provided significant insights into the design and performance of SPR-based sensors. Utilising COMSOL Multiphysics for simulations, a sensor configuration employing a thin film of 45 nm thickness, with a residual cladding of 0.5 µm and an optimized sensing layer width of 10 microns has been successfully modelled. The results for the designs using three different metal thin films (Cu, Ag, and Au) showed that for an analyte RI of 1.42, silver performed best compared to gold and copper, having a wavelength sensitivity of 12,300 $nmRIU^{-1}$, amplitude sensitivity of 1932.51 RIU^{-1}, FWHM of 40 nm, FoM of 307.5 RIU^{-1}, resolution of 8.13×10^{-6} RIU, and DA of 3.075. This is because silver has a low real dielectric constant, which leads to a higher penetration depth of the evanescent field into the analyte region. This allows for a larger interaction volume and, thus, higher sensitivity.

The optimisation of the width and thickness of metal thin film thickness emerged as key factors in achieving a balance between sensitivity and detection accuracy. The sensor's geometry, including D-shape geometry and the design parameters, was found to significantly influence the excitation of plasmonic modes, thus affecting the sensor's sensitivity profile. The outcomes of this research suggest that these sensors could be highly effective for real-time, label-free, and selective detection of various analytes. Moreover, the insights gained from the simulations lay the groundwork for future experimental validation and the potential development of highly sensitive SPR sensor arrays for diverse applications in biochemical and environmental monitoring. The versatility and precision of the proposed sensor design hold promise for significant contributions to the realm of optical fibre sensing technology. Further research may include investigating the performance of the

sensors at a higher analyte refractive index, grid structures, multilayered metal thin film, and optimising the thin film sensing lengths.

Author Contributions: Conceptualization, J.E., R.P. and S.K.; methodology, J.E. and R.P.; software, J.E., R.P. and S.K.; investigation, J.E., R.P. and S.K.; data curation, J.E. and R.P.; writing—original draft preparation, J.E; writing—review and editing, R.P. and S.K.; visualization, J.E., R.P. and S.K.; supervision, R.P. and S.K. All authors have read and agreed to the published version of the manuscript.

Funding: This research received no funding.

Institutional Review Board Statement: Not applicable.

Informed Consent Statement: Not applicable.

Data Availability Statement: The data supporting the findings of this study are available from the corresponding author upon reasonable request.

Acknowledgments: I would like to acknowledge the support provided by the School of Engineering, Robert Gordon University in this research study.

Conflicts of Interest: The authors declare no conflicts of interest.

References

1. Correia, R.; James, S.W.; Lee, S.-W.; Morgan, S.P.; Korposh, S. Biomedical application of optical fibre sensors. *J. Opt.* **2018**, *20*, 073003.
2. Johny, J.; Amos, S.; Prabhu, R. Optical fibre-based sensors for oil and gas applications. *Sensors* **2021**, *21*, 6047.
3. Zeng, S.; Baillargeat, D.; Ho, H.-P.; Yong, K.-T. Nanomaterials enhanced surface plasmon resonance for biological and chemical sensing applications. *Chem. Soc. Rev.* **2014**, *43*, 3426–3452.
4. Bhavsar, K.; Prabhu, R.; Pollard, P. Ultrasensitive graphene coated SPR sensor for biosensing applications. *Opt. Sens.* **2015**, *9506*, 173–178.
5. Nguyen, H.H.; Park, J.; Kang, S.; Kim, M. Surface plasmon resonance: A versatile technique for biosensor applications. *Sensors* **2015**, *15*, 10481–10510.
6. Linman, M.J.; Abbas, A.; Cheng, Q. Interface design and multiplexed analysis with surface plasmon resonance (SPR) spectroscopy and SPR imaging. *Analyst* **2010**, *135*, 2759–2767.
7. Tabasi, O.; Falamaki, C. Recent advancements in the methodologies applied for the sensitivity enhancement of surface plasmon resonance sensors. *Anal. Methods* **2018**, *10*, 3906–3925.
8. Prabowo, B.A.; Purwidyantri, A.; Liu, K. Surface plasmon resonance optical sensor: A review on light source technology. *Biosensors* **2018**, *8*, 80.
9. Shalabney, A.; Abdulhalim, I. Sensitivity-enhancement methods for surface plasmon sensors. *Laser Photonics Rev.* **2011**, *5*, 571–606.
10. Ristau, D.; Ehlers, H. Thin film optical coatings. In *Handbook of Lasers and Optics*; Springer: Berlin/Heidelberg, Germany, 2012.
11. Hinman, S.S.; McKeating, K.S.; Cheng, Q. Surface plasmon resonance: Material and interface design for universal accessibility. *Anal. Chem.* **2018**, *90*, 19.
12. Caucheteur, C.; Guo, T.; Albert, J. Review of plasmonic fiber optic biochemical sensors: Improving the limit of detection. *Anal. Bioanal. Chem.* **2015**, *407*, 3883–3897.
13. Rifat, A.A.; Ahmed, R.; Yetisen, A.K.; Butt, H.; Sabouri, A.; Mahdiraji, G.A.; Yun, S.H.; Adikan, F.M. Photonic crystal fiber based plasmonic sensors. *Sens. Actuators B Chem.* **2017**, *243*, 311–325.
14. Kadhim, R.A.; Abdul, A.K.K.; Yuan, L. Advances in surface plasmon resonance-based plastic optical fiber sensors. *IETE Technol. Rev.* **2022**, *39*, 442–459.
15. Tseng, S.; Chen, C. Side-polished fibers. *Appl. Opt.* **1992**, *31*, 3438–3447.
16. Xie, Q.; Chen, Y.; Li, X.; Yin, Z.; Wang, L.; Geng, Y.; Hong, X. Characteristics of D-shaped photonic crystal fiber surface plasmon resonance sensors with different side-polished lengths. *Appl. Opt.* **2017**, *56*, 1550–1555.
17. Pathak, A.K.; Singh, V.K.; Ghosh, S.; Rahman, B.M.A. Investigation of a SPR based refractive index sensor using a single mode fiber with a large D shaped microfluidic channel. *OSA Contin.* **2019**, *2*, 3008–3018.
18. Ying, Y.; Wang, J.; Hu, N.; Xu, K.; Sun, L.; Si, G. Determination of refractive index using surface plasmon resonance (SPR) and rigorous coupled wave analysis (RCWA) with a D-shaped optical fiber and a nano-gold grating. *Instrum. Sci. Technol.* **2020**, *48*, 376–385.
19. Rafi, H.N.; Kaysir, M.R.; Islam, M.J. Air-hole attributed performance of photonic crystal fiber-based SPR sensors. *Sens. Bio-Sens. Res.* **2020**, *29*, 100364.
20. Rioux, D.; Vallières, S.; Besner, S.; Muñoz, P.; Mazur, E.; Meunier, M. An analytic model for the dielectric function of Au, Ag, and their alloys. *Adv. Opt. Mater.* **2014**, *2*, 176–182.

21. Nahid, E.; Islam, M.J.; Kaysir, M.R.; Hossain, S.S.; Rahman, M.S. Au-strip structure dependent performance investigation of D-shaped SPR sensors for biosensing applications. *Results Opt.* **2023**, *12*, 100460.
22. Kravets, V.G.; Kurioz, P.Y.; Poperenko, L.V. Spectral dependence of the magnetic modulation of surface plasmon polaritons in permalloy/noble metal films. *JOSA B* **2014**, *31*, 1836–1844.
23. White, T.P.; McPhedran, R.C.; de Sterke, C.M.; Botten, L.C.; Steel, M.J. Confinement losses in microstructured optical fibers. *Opt. Lett.* **2001**, *26*, 1660–1662.
24. Nayak, J.K.; Jha, R. Numerical simulation on the performance analysis of a graphene-coated optical fiber plasmonic sensor at anti-crossing. *Appl. Opt.* **2017**, *56*, 3510–3517.
25. Kadhim, R.A.; Yuan, L.; Xu, H.; Wu, J.; Wang, Z. Highly sensitive D-shaped optical fiber surface plasmon resonance refractive index sensor based on Ag-α-Fe_2O_3 grating. *IEEE Sens. J.* **2020**, *20*, 9816–9824.
26. Klantsataya, E.; François, A.; Ebendorff-Heidepriem, H.; Hoffmann, P.; Monro, T.M. Surface plasmon scattering in exposed core optical fiber for enhanced resolution refractive index sensing. *Sensors* **2015**, *15*, 25090–25102.
27. Indhu, A.R.; Keerthana, L.; Dharmalingam, G. Plasmonic nanotechnology for photothermal applications–an evaluation. *Beilstein J. Nanotechnol.* **2023**, *14*, 380–419.
28. Rifat, A.A.; Mahdiraji, G.A.; Chow, D.M.; Shee, Y.G.; Ahmed, R.; Adikan, F.R.M. Photonic crystal fiber-based surface plasmon resonance sensor with selective analyte channels and graphene-silver deposited core. *Sensors* **2015**, *15*, 11499–11510.
29. Rifat, A.A.; Hasan, M.R.; Ahmed, R.; Butt, H. Photonic crystal fiber-based plasmonic biosensor with external sensing approach. *J. Nanophotonics* **2018**, *12*, 012503.
30. Liu, Y.; Li, S.; Chen, H.; Li, J.; Zhang, W.; Wang, M. Surface plasmon resonance induced high sensitivity temperature and refractive index sensor based on evanescent field enhanced photonic crystal fiber. *J. Light. Technol.* **2019**, *38*, 919–928.
31. Yang, X.; Lu, Y.; Wang, M.; Yao, J. An exposed-core grapefruit fibers based surface plasmon resonance sensor. *Sensors* **2015**, *15*, 17106–17114.
32. Kaur, V.; Singh, S. D-shaped photonic crystal fiber based surface plasmon resonance sensor using dual coating of metal oxide for healthcare applications. In Proceedings of the 2021 IEEE 16th Nanotechnology Materials and Devices Conference (NMDC), Vancouver, BC, Canada, 12–15 December 2021.
33. Tong, K.; Wang, F.; Wang, M.; Dang, P.; Wang, Y.; Sun, J. D-shaped photonic crystal fiber biosensor based on silver-graphene. *Optik* **2018**, *168*, 467–474.
34. Popescu, V.A.; Puscas, N.N.; Perrone, G. Simulation of the sensing performance of a plasmonic biosensor based on birefringent solid-core microstructured optical fiber. *Plasmonics* **2017**, *12*, 905–911.